International Journal of Heat and Fluid Flow 30 (2009) 1114–1128

Contents lists available at ScienceDirect

International Journal of Heat and Fluid Flow

journal homepage: www.elsevier.com/locate/ijhff

Numerical investigation of forced convection heat transfer in unsteady flow past a row of square cylinders

Dipankar Chatterjee [a], Gautam Biswas [b,*], Sakir Amiroudine [c]

[a] LPMI, Arts et Métiers Paris Tech, 2 Boulevard du Ronceray, BP 93525, 49035 Angers, Cedex 01, France
[b] Department of Mechanical Engineering, Indian Institute of Technology, Kanpur, Kanpur 208 016, India
[c] Laboratoire TREFLE UMR CNRS 8508, Esplanade des Arts et Métiers 33405, Talence Cedex, France

ARTICLE INFO

Article history:
Received 13 March 2009
Received in revised form 7 September 2009
Accepted 15 September 2009

Keywords:
Multiple bluff bodies
Square cylinders
Vortex shedding
Unsteady periodic flow
Forced convection heat transfer
Cylinder interaction frequency

ABSTRACT

This paper presents the unsteady laminar forced convection heat transfer from a row of five isothermal square cylinders placed in a side-by-side arrangement at a Reynolds number of 150. The numerical simulations are performed using a finite volume code based on the PISO algorithm in a collocated grid system. Special attention is paid to investigate the effect of the spacing between the cylinders on the overall transport processes for the separation ratios (spacing to size ratio) between 0.2 and 10. No significant interaction between the wakes is observed for spacing greater than four times the diameter at this Reynolds number. However, at smaller spacing, the wakes interact in a complicated manner resulting different thermo-hydrodynamic regimes. The vortex structures and isotherm patterns obtained are systematically presented and discussed for different separation ratios. In addition, the mean and instantaneous drag and lift coefficients, mean and local Nusselt number and Strouhal number are determined and discussed for various separation ratios. A new correlation is derived for mean Nusselt number as a function of separation ratio for such flows.

1. Introduction

The forced convection heat transfer around multiple bluff bodies has wide engineering applications such as heat exchangers, space heating, cooling towers, chimneys, power generators, heat losses from high-rise buildings and other thermal applications. The most striking phenomenon during the flow past multiple bluff bodies is the generation of a complex flow structure as a consequence of the mutual interactions among the wakes behind the bodies. These wake interactions subsequently lead to the complex vortex shedding phenomena. The forced convection heat transfer and the resulting thermal field is dictated by this complex flow structure. A thorough knowledge of the vortex shedding mechanism is required for better understanding heat transfer in the wakes which is essential for the development of many engineering equipment.

Numerous attempts have been made for modeling the fluid flow and heat transfer over a single circular and/or square cylinder. Additionally, there are many reported work on flow and heat transfer over multiple circular cylinders with various arrangements. Excellent and extensive reviews of the pertinent hydrodynamic studies are available in Zdravkovich (1997, 2003) whereas the thermal aspects can be found in Morgan (1975) and Suzuki and Suzuki (1994). However, there is a real scarcity in the literature for the coupled fluid flow and heat transfer over multiple square cylinders and to the best of the authors' knowledge, there is no reported work on the forced convection heat transfer over a row of square cylinders at low Reynolds number. It needs to be emphasized at this point that the flow patterns and the wake structures for the cases of flow over row of square cylinders are considerably different from that over a row of circular cylinders because of the fact that unlike the circular cylinders the square cylinders tend to fix the separation point, causing differences in the critical regimes. Furthermore, the separation mechanisms depending on the shedding frequencies and the aerodynamic forces also differ significantly for the two geometries.

In the context of flow over a row of square cylinders, Mizushima and Takemoto (1996) performed flow visualization of the pattern downstream of a row of square cylinders. They found for a specific Reynolds number and s/d combinations, both flopping and bistable flip-flop behavior downstream of the cylinders. Kolar et al. (1997) performed measurements on a pair of square cylinders using laser Doppler velocimetry at $Re = 23100$ and $s/d = 2$. They examined the strengths of the vortices both near the gap and in the outer shear layers. It is worth mentioning that their results confirmed the dominant existence of anti-phase synchronized pattern in the flow. Valencia and Cid (2002) numerically investigated

* Corresponding author. Tel.: +91 512 2597656; fax: +91 512 2597408.
E-mail address: gtm@iitk.ac.in (G. Biswas).

0142-727X/$ - see front matter © 2009 Elsevier Inc. All rights reserved.
doi:10.1016/j.ijheatfluidflow.2009.09.004

Nomenclature

C_D	drag coefficient
C_L	lift coefficient
$\overline{C_D}$	mean drag coefficient
d [m]	cylinder size
f [Hz]	frequency of vortex shedding
F_D [N]	drag force
F_L [N]	lift force
g [m/s^2]	acceleration due to gravity
G_r	Grashof number $= g\beta(T_W - T_\infty)d^3/\nu^2$
h [W/m^{2}K]	local heat transfer coefficient
k [W/mK]	thermal conductivity of fluid
L_i [m]	upstream length
L_o [m]	downstream length
L_x [m]	length of computational domain
L_y [m]	width of computational domain
Nu	local Nusselt number
$\overline{Nu}$	time average Nusselt number
n	normal direction
p	pressure
Pr	Prandtl number = ν/α
Re	reynolds number $= u_\infty d/\nu$
Ri	richardson number $= Gr/Re^2$
s [m]	separation length
St	Strouhal number $= fd/u_\infty$
t	time
T [K]	temperature
T_f [K]	film temperature $= (T_W + T_\infty)/2$
T_W [K]	cylinder surface temperature
T_∞ [K]	free stream temperature
u	axial velocity
u_∞ [m/s]	free stream velocity
v	normal velocity
x, y	axial and normal coordinates of the system

Greek symbols

α [m^2/s]	thermal diffusivity of fluid
β [1/K]	thermal coefficient of volume expansion
θ	temperature
λ_{CD}	mean amplitude of drag coefficient signals
ν [m^2/s]	kinematic viscosity of fluid
ρ [kg/m^3]	density of fluid
τ	period of vortex shedding
φ [°]	phase difference between lift coefficient signals

Subscripts

W	cylinder surface
∞	free stream

Superscript

–	dimensional quantity

the unsteady turbulent flow and heat transfer in a channel with stream-wise periodically mounted square bars arranged side-by-side to the approaching flow for a Reynolds number of 2×10^4. Mizushima and Akinaga (2003) investigated experimentally and also numerically the interactions of wakes for the flow past a row of square and circular bars. Their results showed that at $s/d = 1$, in-phase vortex shedding occurred between cylinders whereas at $s/d = 3$, anti-phase shedding was observed. Agrawal

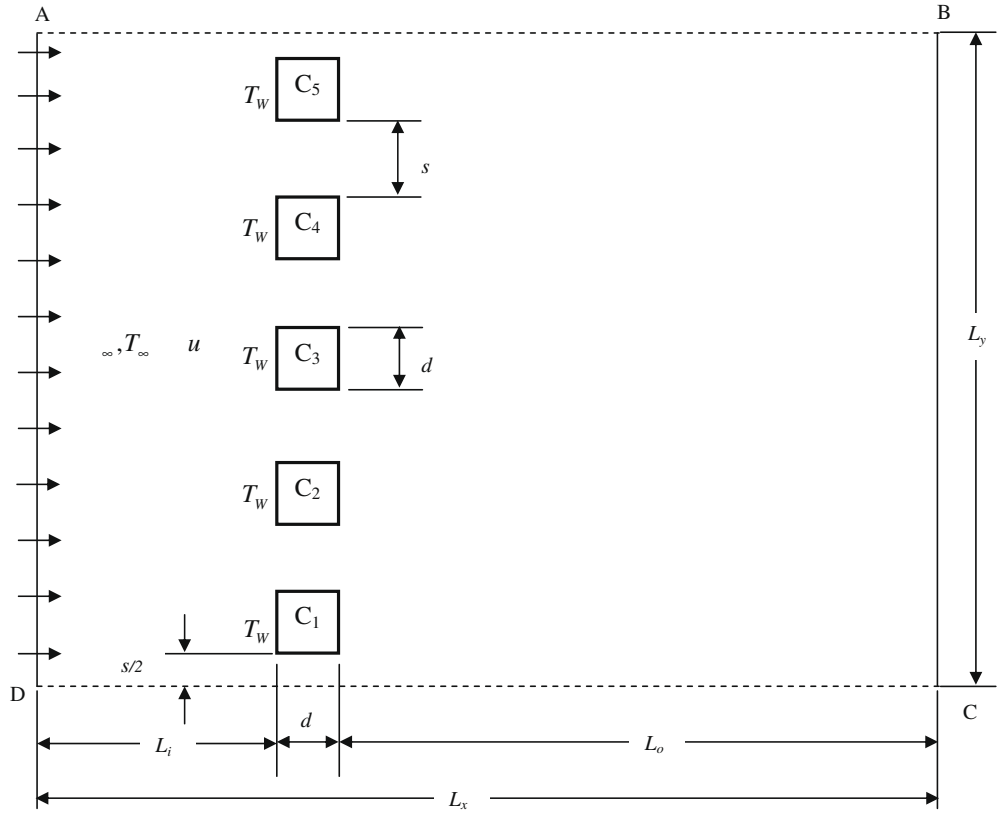

Fig. 1. Schematic diagram of the computational domain. The size of the computational domain is ($L_x = L_i + d + L_o = 38\ d$, $L_y = 5\ (s + d)$).

et al. (2006) performed numerical study of flow around a pair of square cylinders. They showed the presence of synchronized and chaotic regimes at $Re = 73$, in agreement with the well known results for circular cylinders. Inoue et al. (2006) analyzed flow past two square cylinders placed in side-by-side arrangement in a uniform flow. They also studied the mechanism of sound generation. In another article, Inoue and Suzuki (2007) explained the mechanism of sound generation from three side-by-side square cylinders and the effect of spacing between them. Kumar et al. (2008) conducted two-dimensional simulations to understand the dynamics of vortices in a flow around nine square cylinders placed in a side-by-side arrangement for s/d ratio ranging from 0.3 to 12. They deployed lattice Boltzmann method in the low Reynolds number regime ($Re = 80$). Three distinct flow regimes such as synchronized, quasi-periodic and chaotic were observed for $s/d < 6$ from their study. In a very recent article, Sewatkar et al. (2009) studied the combined effect of cylinder spacing and Reynolds number on the flow across a row of nine square cylinders for $30 \leqslant Re \leqslant 140$ and $1 \leqslant s/d \leqslant 4$ using the same lattice Boltzmann technique. Apart from confirming the various flow regimes obtained by Kumar et al. (2008), they also computed the critical Reynolds numbers at which the transition from steady to unsteady flow takes place for each s/d ratio through a bifurcation diagram. In another recent paper, Chatterjee et al. (2009) demonstrated the effect of cylinder spacing on vortex dynamics for flow over a row of five in-line square cylinders in an infinite medium at $Re = 150$ and for $s/d = 1.2$, 2, 3 and 4 using a finite volume method.

From the above discussion, it is well understood that although there are many reported work on the hydrodynamic aspects, the corresponding thermal studies are almost unavailable. Furthermore, the studies pertaining to the row of square cylinders are actually very less and there is very little documentation and limited quantitative information for the different flow regimes evolving as a result of wake interactions during flow over a row of square cylinders. Accordingly, our aim of the present work is to numerically investigate the thermo-hydrodynamic phenomena for Newtonian fluid flow around multiple isothermal square cylinders placed in a side-by-side arrangement, at a low Reynolds number. A row of five identical cylinders are chosen here in an infinite medium. The effect of cylinder spacing on fluid flow and heat transfer is investigated by varying the separation ratio. A finite volume method is used to simulate and analyze this important problem.

2. Description of the problem, governing equations and boundary conditions

The problem under consideration is shown schematically in Fig. 1. Five fixed identical square cylinders with sides (d) are kept in a side-by-side arrangement and exposed to a constant free stream with uniform velocity u_∞ and temperature T_∞ respectively. The cylinders are also heated to a constant temperature T_W ($>T_\infty$). The spacing (s) between two successive cylinders is identical. The effect of cylinder spacing on the overall transport mechanism is analyzed for spacing to diameter ratio of 0.2, 0.4, 0.8, 1.2, 2, 3, 4, 6, 8 and 10. The Reynolds numbers is kept low ($Re = 150$) for this study in order to restrict the study to the 2D flow.

The dimensionless governing equations for this two-dimensional, unsteady, laminar, incompressible and Newtonian fluid flow with constant fluid properties can be expressed in the following conservative forms:

1. Continuity:

$$\frac{\partial u}{\partial x} + \frac{\partial v}{\partial y} = 0 \tag{1}$$

2. Momentum:

$$\frac{\partial u}{\partial t} + \frac{\partial (uu)}{\partial x} + \frac{\partial (uv)}{\partial y} = -\frac{\partial p}{\partial x} + \frac{1}{Re}\left(\frac{\partial^2 u}{\partial x^2} + \frac{\partial^2 u}{\partial y^2}\right) \tag{2a}$$

$$\frac{\partial v}{\partial t} + \frac{\partial (uv)}{\partial x} + \frac{\partial (vv)}{\partial y} = -\frac{\partial p}{\partial y} + \frac{1}{Re}\left(\frac{\partial^2 v}{\partial x^2} + \frac{\partial^2 v}{\partial y^2}\right) + Ri\theta \tag{2b}$$

3. Energy:

$$\frac{\partial \theta}{\partial t} + \frac{\partial (u\theta)}{\partial x} + \frac{\partial (v\theta)}{\partial y} = \frac{1}{RePr}\left(\frac{\partial^2 \theta}{\partial x^2} + \frac{\partial^2 \theta}{\partial y^2}\right) \tag{3}$$

where u, v are the velocity components along x and y directions of a Cartesian coordinate system respectively, t is the time, p is the pressure, Re ($=u_\infty d/\nu$) is the Reynolds number based on the cylinder dimension, Ri ($=Gr/Re^2$) is the Richardson number, Gr is the Grashof number, θ is the temperature and $Pr = \nu/\alpha$ is the Prandtl number. For

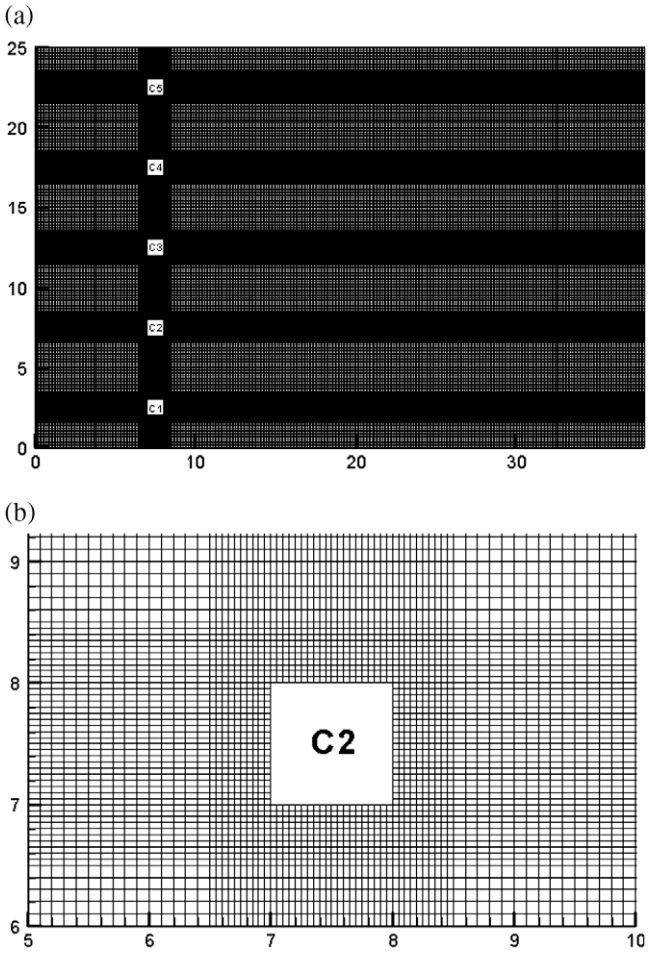

Fig. 2. A representative grid distribution for $s/d = 4$: (a) computational domain and (b) a closer view around a cylinder.

Table 1
Grid distributions for different s/d ratio.

s/d	$L_x \times L_y$
0.2	400 × 120
0.4	400 × 140
0.8	400 × 180
1.2	400 × 220
2.0	400 × 250
3.0	400 × 330
4.0	400 × 350

the present study, $Ri = 0$ and $Pr = 0.71$. The fluid properties are described by the density ρ, kinematic viscosity ν and thermal diffusivity α. All the fluid properties are considered at some artificial temperature, the so-called "film" temperature T_f, which is defined by the arithmetic mean of the cylinder wall T_W and the free stream temperature T_∞ as $T_f = (T_W + T_\infty)/2$. The dimensionless variables are defined as:

$$u = \frac{\overline{u}}{u_\infty}, \quad v = \frac{\overline{v}}{u_\infty}, \quad x = \frac{\overline{x}}{d}, \quad y = \frac{\overline{y}}{d}, \quad p = \frac{\overline{p}}{\rho u_\infty^2},$$
$$t = \frac{u_\infty \overline{t}}{d}, \quad \theta = \frac{T - T_\infty}{T_W - T_\infty} \tag{4}$$

The boundary conditions of interest in this study are as follows. At the inlet (face AD in Fig. 1), which is located $L_i = 7d$ upstream of

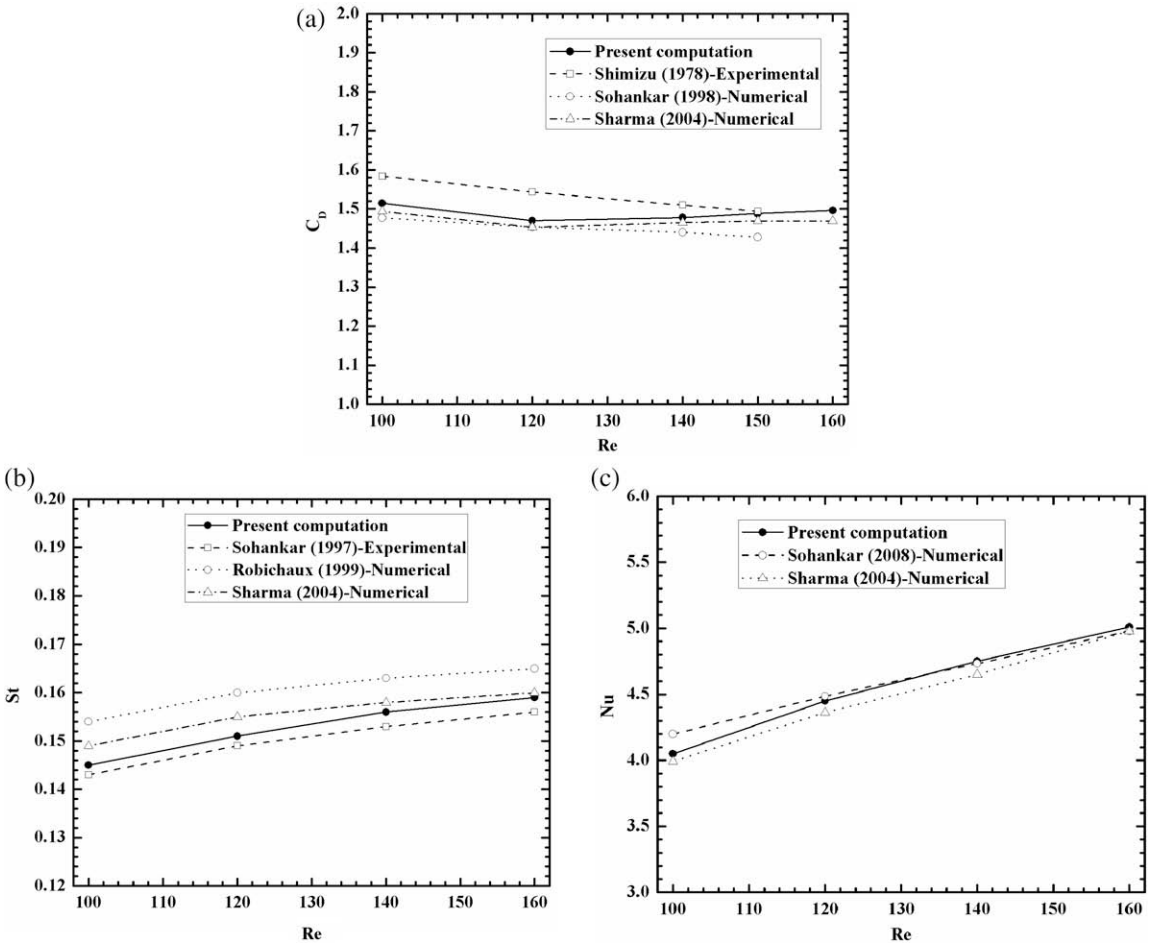

Fig. 3. Variation of (a) total drag coefficient, (b) Strouhal number and (c) Nusselt number as a function of Reynolds number for single square cylinder.

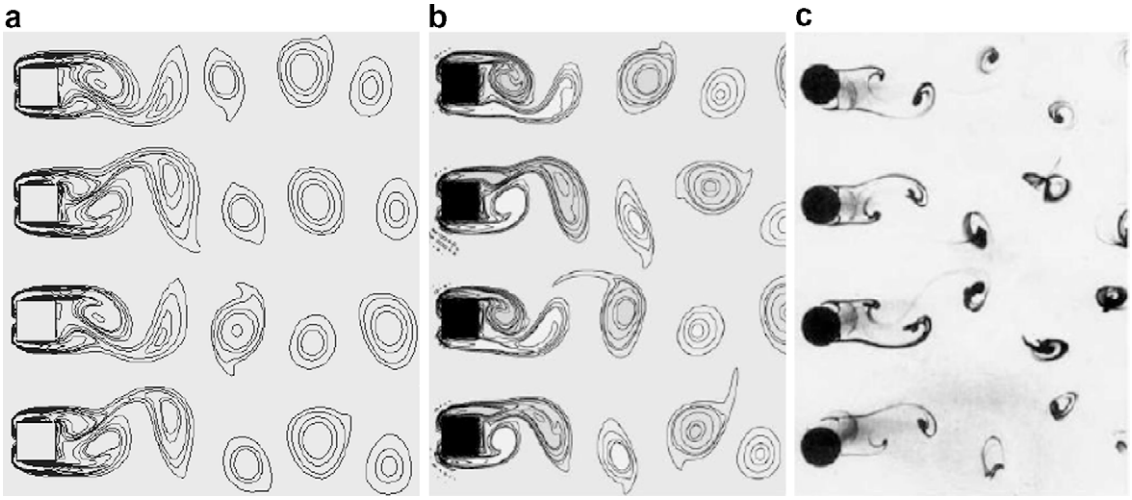

Fig. 4. Comparison of wake structure from a row of cylinders ($s/d = 2$, $Re = 200$). (a) Present simulation, (b) numerical simulation of Kumar et al. (2008) and (c) experiments of Kobayashi (1984).

the row of cylinders, a uniform flow of constant temperature is prescribed:

$$u = 1, \quad v = 0, \quad \theta = 0 \tag{5}$$

At the outlet (face BC in Fig. 1), which is located at $L_0 = 30d$ downstream of the row of cylinders, an outflow boundary condition is given, i.e.,

$$\frac{\partial u}{\partial x} = \frac{\partial v}{\partial x} = \frac{\partial \theta}{\partial x} = 0 \tag{6}$$

Although this boundary condition is strictly valid only when the flow is fully developed, its use in other flow conditions is also permissible for computational convenience provided that the outlet boundary is located sufficiently far downstream from the region of interest.

A periodic boundary condition has been prescribed on the lateral faces (AB and DC in Fig. 1) of the computational domain for extending the results to an infinite number of cylinders. The boundary condition on the cylinder surfaces is given by:

$$u = v = 0, \quad \theta = 1 \tag{7}$$

The flow is assumed to start impulsively from rest.

The lift and drag coefficients are computed from:

$$C_L = C_{LP} + C_{LV} = \frac{2F_L}{\rho u_\infty^2 d} \tag{8}$$

$$C_D = C_{DP} + C_{DV} = \frac{2F_D}{\rho u_\infty^2 d} \tag{9}$$

where C_{LP} and C_{LV} represent the lift coefficients due to pressure and viscous forces respectively, similarly C_{DP} and C_{DV} represent the drag coefficients due to pressure and viscous forces. F_L and F_D are the lift and drag forces respectively acting on the cylinder surface. Thus the lift and drag coefficients due to viscous force and pressure force can be obtained from the following expressions:

$$C_{LP} = 2\int_0^1 (p_b - p_t)dx, \quad C_{LV} = \frac{2}{Re}\int_0^1 \left[\left(\frac{\partial v}{\partial x}\right)_f + \left(\frac{\partial v}{\partial x}\right)_r\right]dy \tag{10}$$

$$C_{DP} = 2\int_0^1 (p_f - p_r)dy, \quad C_{DV} = \frac{2}{Re}\int_0^1 \left[\left(\frac{\partial u}{\partial y}\right)_b + \left(\frac{\partial u}{\partial y}\right)_t\right]dx \tag{11}$$

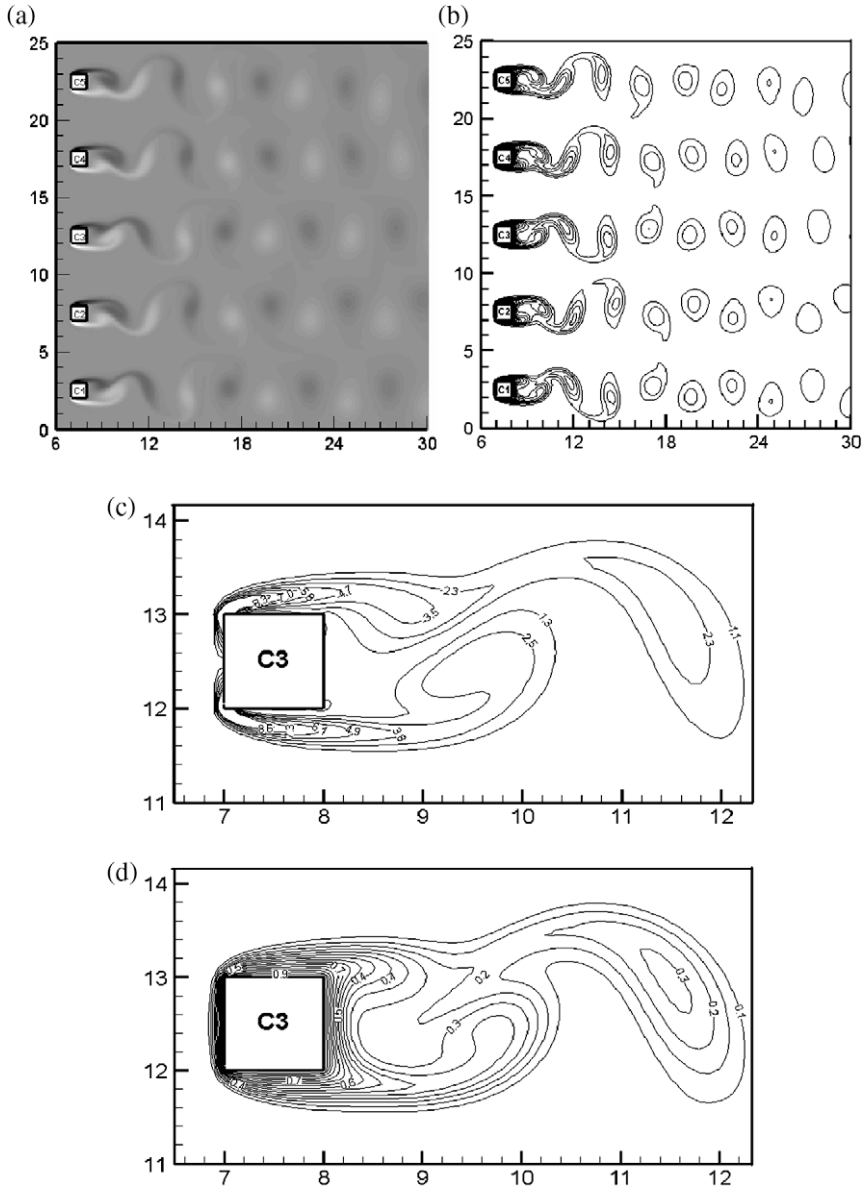

Fig. 5. (a) Instantaneous vorticity and (b) isotherm contours, (c) closer view of iso-vorticities and (d) closer view of isotherms. All contours are plotted for the case of $s/d = 4$.

The subscripts *f*, *r*, *b* and *t* refer to the front, rear, bottom and top surfaces of the cylinders. The Strouhal number, which characterizes the periodicity in a flow field, is defined as $St = fd/u_\infty$ where *f* is the vortex shedding frequency.

The heat transfer between the cylinder and the surrounding fluid is calculated from the Nusselt number. The local Nusselt number based on the cylinder dimension is calculated using the following equation:

$$Nu = \frac{hd}{k} = -\frac{\partial\theta}{\partial n} \tag{12}$$

where *h* is the local heat transfer coefficient, *k* is the thermal conductivity of the fluid and *n* is the direction normal to the cylinder surface. Surface average heat transfer at each face of the cylinder is obtained by integrating the local Nusselt number along the cylinder face. The time dependent total average cylinder Nusselt number is the total of the average Nusselt number at each face of the cylinder. The time average local Nusselt number is obtained by integrating the local Nusselt number over a large period of time.

3. Method of solution

The conservation equations subjected to the aforementioned boundary conditions are solved using a finite volume based method according to the Pressure Implicit with Splitting of Operators

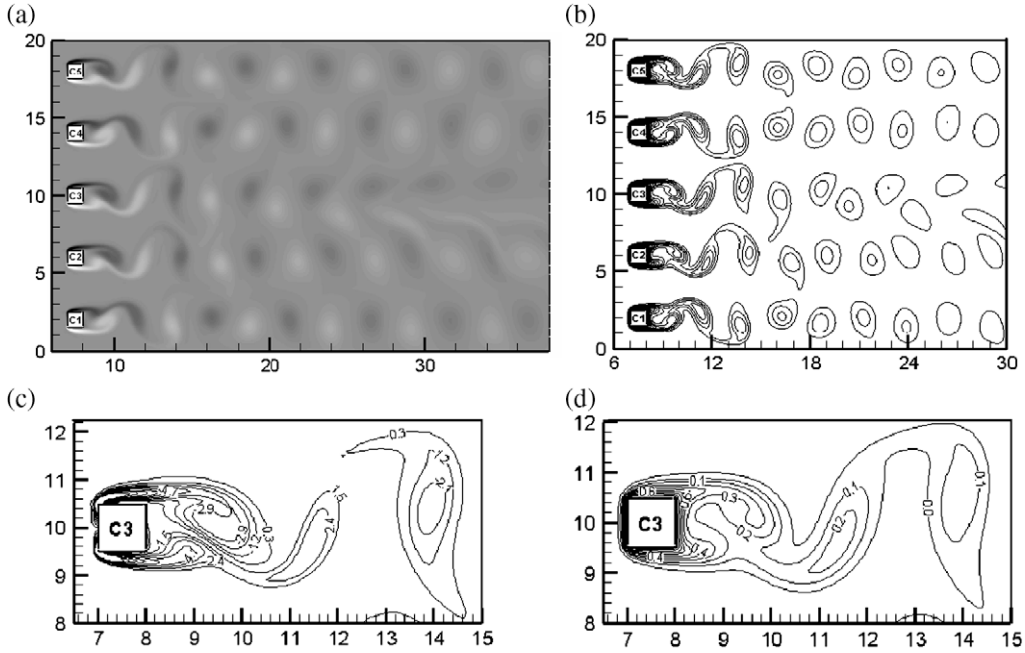

Fig. 6. (a) Instantaneous vorticity and (b) isotherm contours, (c) closer view of iso-vorticities and (d) closer view of isotherms. All contours are plotted for the case of *s*/*d* = 3.

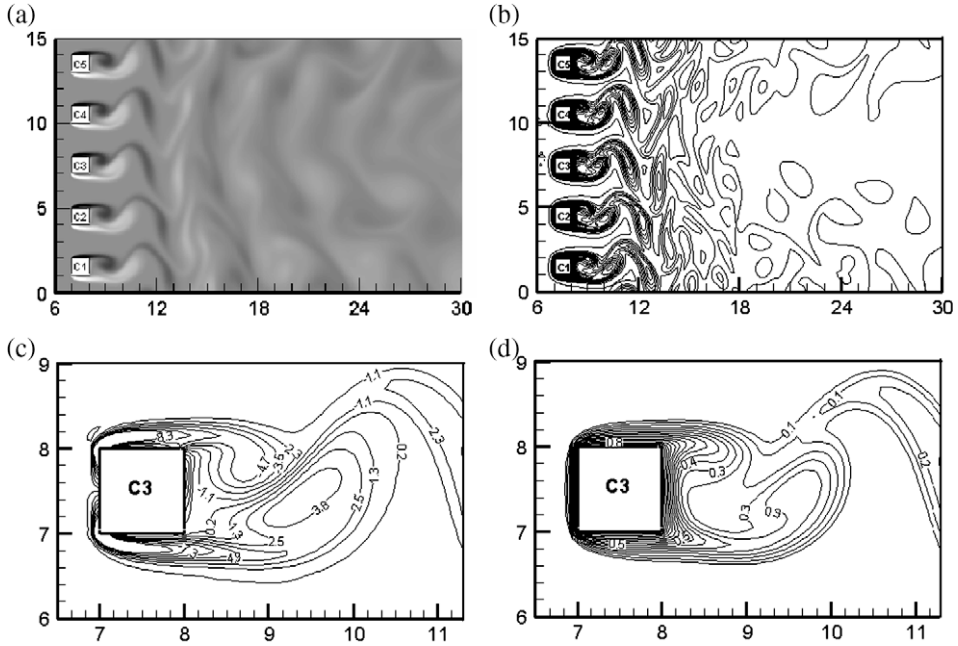

Fig. 7. (a) Instantaneous vorticity and (b) isotherm contours, (c) closer view of iso-vorticities and (d) closer view of isotherms. All contours are plotted for the case of *s*/*d* = 2.

(PISO) algorithm (Issa, 1986). The PISO algorithm is chosen here for its robust convergence behavior for unsteady problems. A second order accurate upwind scheme for discretizing the convection–diffusion terms of the momentum equations as well as energy equation and a second order accurate implicit Adams–Bashforth scheme for time marching are used. The conditions necessary to prevent numerical oscillations are determined from the Courant–Friedrichs–Lewy (CFL) and the grid Fourier criteria (Mukhopadhyay et al., 1992). The final time step size is taken as the minimum of the two criteria mentioned above. In the numerical solution a time step size of 0.008 is used satisfying the above restrictions.

The number of grid points and their distribution is an important issue in such transient flows over multiple cylinders because of the associated complexity in the flow as well as the separation and vortex shedding. The simulation domain is discretized accordingly by a non-uniform grid with a finer grid distribution near the cylinders to capture the viscous boundary layer as well as the wake and the vortex street behind the cylinders. A representative grid distribution for the case of $s/d = 4$ is shown in Fig. 2. Fig. 2a shows the grid distribution in the entire computational domain, whereas, a closer view near one cylinder (C_2) is depicted in Fig. 2b. Table 1 shows the grids used for different s/d ratios.

In order to validate the present numerical code, the fluid flow and heat transfer around a single square cylinder are studied and the results obtained are compared with the available results in the literature (Shimizu and Tanida, 1978; Sohankar et al., 1997, 1998; Sharma and Eswaran, 2004; Robichaux et al., 1999; Sohankar and Etminan, 2008). This is because, there are no experimental or numerical results reported in the literature for the physical problem configuration with the Reynolds number and the boundary conditions considered for the present study. Fig. 3a–c demonstrates the comparison of the present computation with the existing results in terms of the variation of total drag coefficient, Strouhal number and Nusselt number at various Reynolds numbers for flow

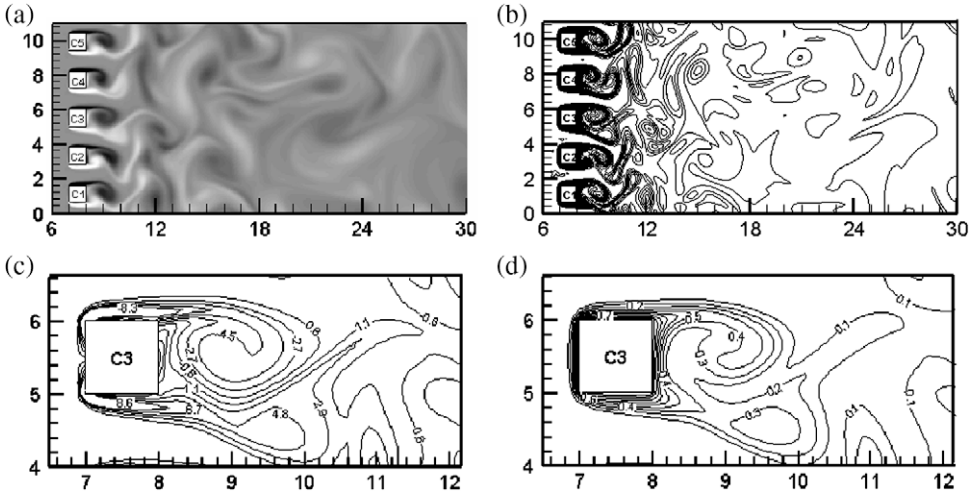

Fig. 8. (a) Instantaneous vorticity and (b) isotherm contours, (c) closer view of iso-vorticities and (d) closer view of isotherms. All contours are plotted for the case of $s/d = 1.2$.

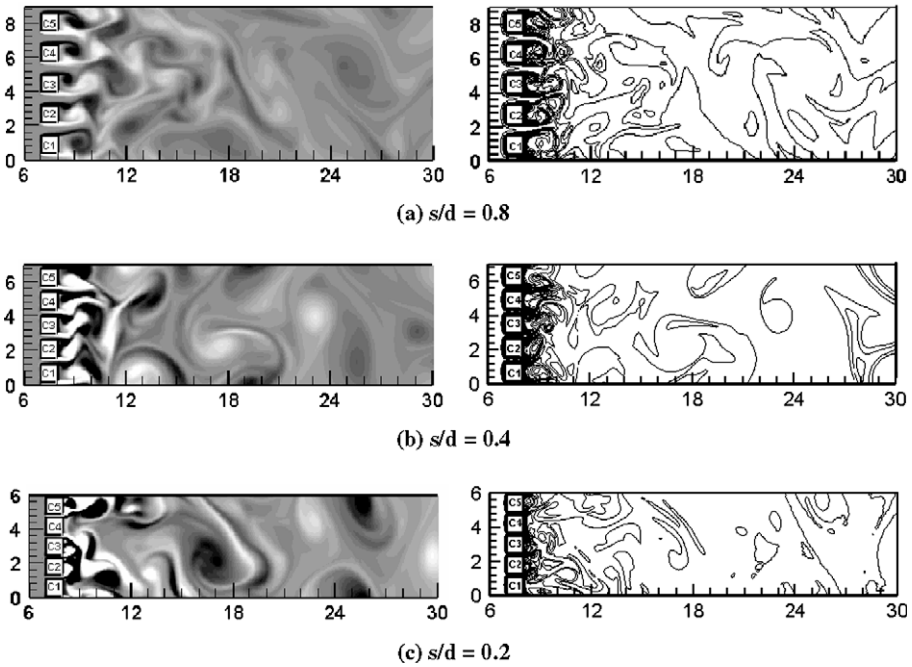

Fig. 9. Instantaneous vorticity (left) and isotherm (right) contours for $s/d < 1$.

over a single square cylinder. A reasonable agreement is found between the present simulation and the reported results. However, the small deviation (within 5%) can be attributed by the use of different grid sizes, time steps and solution algorithms. Further, the flow structures for a row of cylinders as obtained numerically by Kumar et al. (2008) and experimentally by Kobayashi (1984) are compared with the present simulation in Fig. 4. Although the size and shape of the cylinders are different, still a good qualitative agreement is found in terms of the vortex structures downstream the cylinders.

4. Results and discussion

4.1. Flow structures and isotherm patterns

The flow structures and isotherm patterns are presented here systematically for different s/d ratios. All the results are presented after having reached the dynamical steady state. The computation is first carried out with the separation ratio $s/d = 10$ and then successively reduced. Almost no interaction between the wakes is found for separation ratios $s/d = 10$, 8 and 6 which is justified by

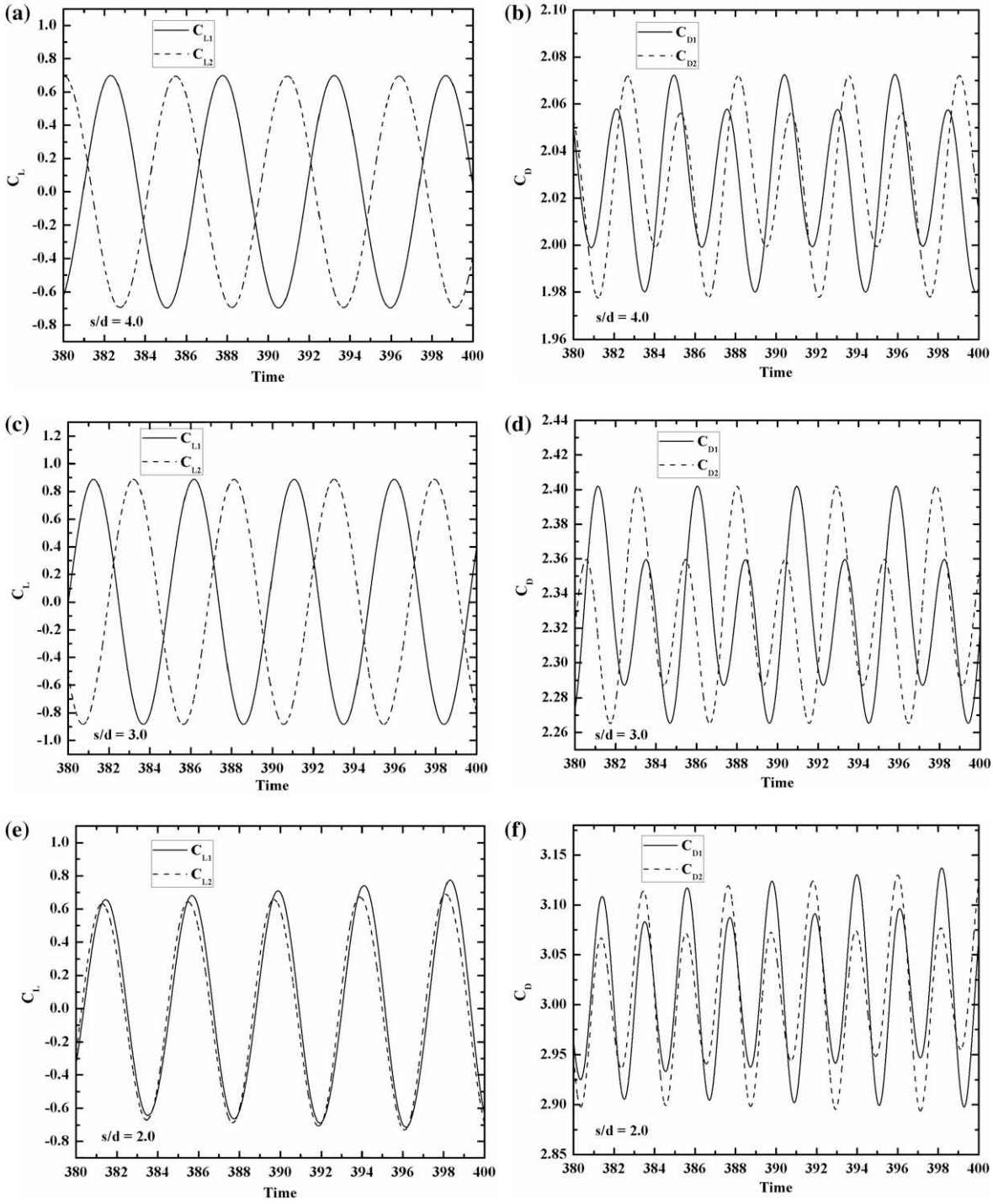

Fig. 10. Time signals of lift (left) and drag (drag) coefficients for $s/d = 4$, 3 and 2.

the fact that the mean drag coefficient, Strouhal number and mean Nusselt number have nearly constant values at these separation ratios. Similar observations are also reported in Kumar et al. (2008). Because of this insignificant interaction in the flow and isotherm patterns, less attention is paid to investigate the transport phenomena in greater detail at those separation ratios. However, for the configurations with $s/d \leqslant 4$, the wakes behind the cylinders interact in a complicated fashion resulting in a variety of thermo-hydrodynamic fields.

Fig. 5 demonstrates the instantaneous vorticity contours and isotherms for the configuration with $s/d = 4$. A synchronized shedding pattern is observed in which some of the vortices are in in-phase and some others in anti-phase. For example, the vortex shedding from cylinders C_1 and C_2 are observed to be in anti-phase, so also are the shedding from cylinders C_3 and C_4. The shedding from C_2, C_4 and C_5 are synchronized in-phase. The vortices can be clearly visible and also they remain distinct throughout the computational domain without significant lateral spread. This can be attributed to weakly interactive flow pattern arising out of relatively larger spacing between the cylinders. This result is in good agreement with the experimental observation of Williamson (1985) for two circular cylinders with $s/d = 3$ and $Re = 100$. Sumner et al. (1999) and Zhou et al. (2000) had also similar observations. It is to be mentioned here that since both the vorticity and thermal energy are transported by the flow itself, the vorticity contours as well as the isotherms exhibit similar features. The isotherms are seen to be crowded around the cylinders as shown in Fig. 5b. The crowding of isotherms are precisely more on the front face of the cylinders compared to the top, bottom and rear faces as demonstrated in the closer view of Fig. 5d. This indicates a higher heat transfer characteristic at the front face. This phenomenon can be physically justified by looking into the closer view of the corresponding vorticity contour in Fig. 5c. The effect of flow separation can be seen from this figure which in turn is responsible for less heat transfer in the rear faces of the cylinders.

The instantaneous vorticity contours and isotherms for the configuration with $s/d = 3$ are shown in Fig. 6a–d. The vortices are again clearly apparent like the previous case of $s/d = 4$. Fig. 6a shows that the shedding from C_1 and C_2 are in anti-phase and those from C_3 and C_4 are also in anti-phase. It is interesting to note that the vortices from C_4 and C_5 are in anti-phase. As a result, the shedding from C_2 and C_3 are in in-phase. One can see that there is some evidence of merging of vortices at far downstream locations (close to the exit of the domain). The vortex shedding from one cylinder seems to have a definite phase relationship with the shedding from other cylinders. The energy is transported in a similar fashion by the fluid flow to the downstream region. The isotherms are once again crowded towards the front face signifying greater heat transfer coefficient as depicted in Fig. 6d, which is a consequence of the flow separation behind the cylinders (refer to Fig. 6c).

Fig. 7a–d illustrates instantaneous wake structures and isotherm patterns for $s/d = 2$. The wake reveals in-phase synchronized pattern as can be seen from Fig. 7a. The flow behavior is in qualitative agreement with the results of Inoue and Suzuki (2007). Shedding is in-phase because vortices of same color (contours) corresponding to shedding from the side-by-side cylinders are at approximately the same streamwise locations. The vortices do not remain distinct downstream the computational domain, because of strong interactions due to relatively small spacing between the cylinders. The isotherms for $s/d = 2$ are shown in Fig. 7b with a closer view in Fig. 7d. In the perspective of Fig. 7c, the isotherm patterns are self explanatory.

The flip-flopping pattern is seen for configuration with $s/d = 1.2$. Fig. 8a–d illustrates the instantaneous vorticity contours and isotherms for $s/d = 1.2$. The structures of vortices are smaller than

Table 2
Variation of global quantities with s/d.

s/d	λ_{CD}	φ (°)	τ	St
4	2.02	200	5.6	0.178
3	2.26	190	5.0	0.20
2	3.0	0	4.4	0.227

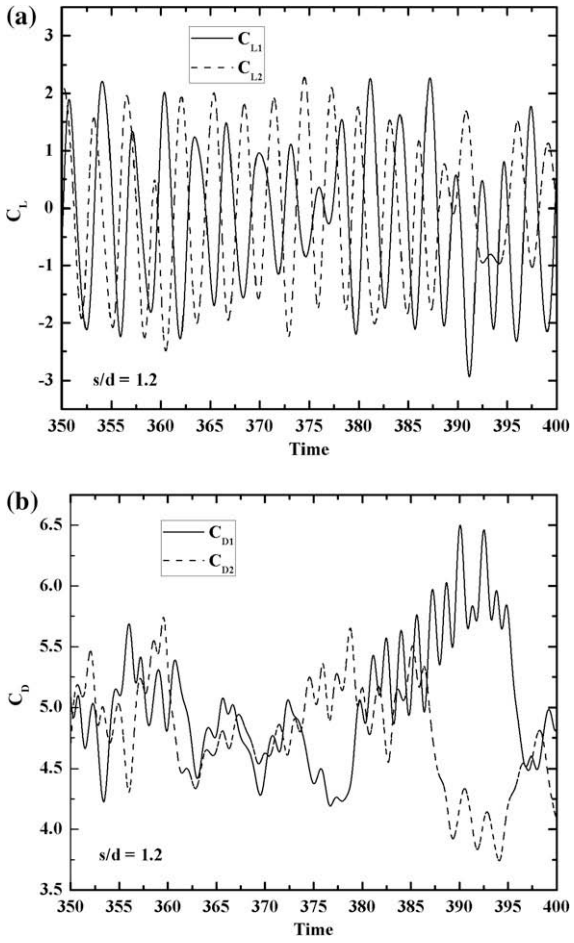

Fig. 11. Time signals of (a) lift and (b) drag coefficient for $s/d = 1.2$.

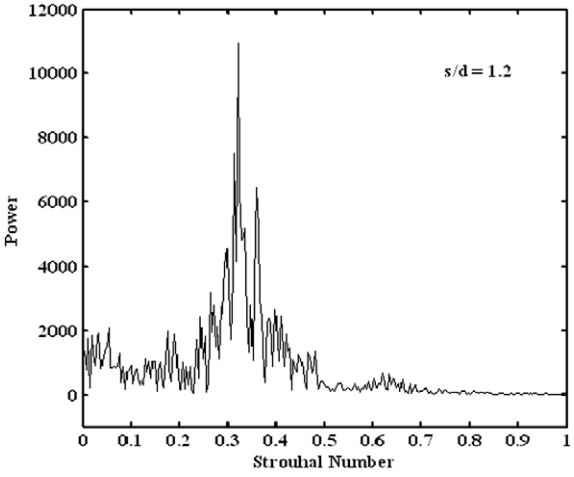

Fig. 12. Power spectra of lift coefficient signal for $s/d = 1.2$.

the vortical structures observed in the earlier cases. This can be attributed to the fact that the flow interference between successive cylinders is quite strong at this small separation ratio and consequently oscillating regions are found to exist together. The flow in this case can be characterized by the jets in the gaps between consecutive cylinders and these jets interact is such a way that the structures diffuse downstream. For a jet, the fluid particles in the ambient are set in motion due to interfacial shear. This has an effect of enlarging the jet width. Consequently, this process may be viewed as one of mass transfer from the surroundings to the jet, namely the jet has entrained fluid from the neighborhood. In the near wake of an individual cylinder, the velocity profile shows a deficit (in a time-averaged sense) and the entrainment is from the outer flow into the wake. Thus, the velocity deficit gradually diminishes with distance away from the cylinder. The wake size increases in the transverse direction, if the entrainment is more from outer region into the wake. In the near wake, two additional mechanisms become important. First, the pressure within the wake is considerably smaller than that outside and results in a rapid recovery of the velocity profile. On the other hand, a second factor that originates from the time-dependent oscillations relates to bursts of fluid from the central core of the wake to the surrounding fluid. For the multiple cylinders, such attributes combine via additive effects. It also reveals sporadic events when two or more

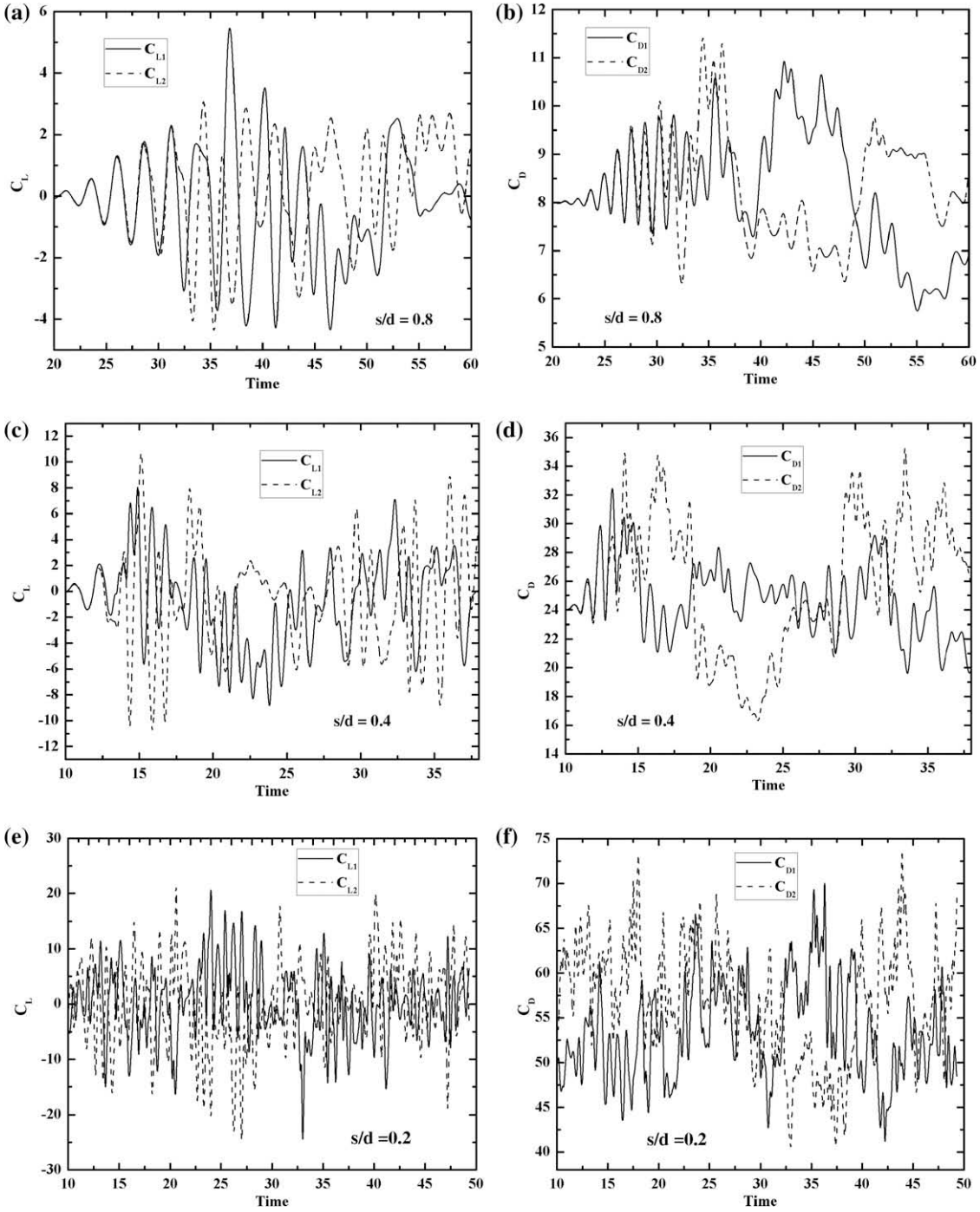

Fig. 13. Time signals of lift (left) and drag (right) coefficients for $s/d < 1$.

vortical fluid lumps merge to form a single lump. The flow behavior is very much similar to the experimental results of Bradshaw (1965) with circular cylinders at $Re = 1500$ and near similar spacing. Our wake structure is quite identical with that was observed by Kumar et al. (2008) using nine square cylinders and $s/d = 1$ at $Re = 80$.

Fig. 9a–c represents the instantaneous vorticity and isotherm plots for $s/d < 1$. Here the flow behavior is completely dominated by the jets produced between the cylinders and the resulting flow becomes chaotic downstream. Although the flow fields for these separation ratios seem to be qualitatively similar to that at $s/d = 1.2$, important differences exist for the cases pertaining to $s/d < 1$. The vortices are no longer distinct even at the near wake of the cylinders and some of them are seen to be substantially smaller than the normally shed vortices. This becomes more prominent at very small separation ratio, e.g. $s/d = 0.2$. The jets interact with the shed vortices and accordingly, in addition to the natural frequency of vortex shedding and the jet-induced frequency, "combined frequencies" arise due to the interaction of these multiple frequencies. As a result of this chaotic nature of the flow field, the corresponding temperature field reveals better mixing.

4.2. Global quantities

Fig. 10a–f shows the time series of lift and drag coefficients of two consecutive cylinders (for example C_1 and C_2) for $s/d = 4$, 3 and 2. It can be observed from the figures that both lift and drag coefficients are sinusoidal in nature. The amplitude of C_L remains constant with a zero mean, whereas the amplitude of C_D is observed to oscillate. The frequency of oscillation of the instantaneous C_L is half of that of the instantaneous C_D. There is a definite phase difference between C_{L1} and C_{L2}, whereas the drag coefficients are approximately in-phase. Generally following phenomena are observed during low Reynolds number flow past a bluff body. At low Reynolds numbers (in the range of 150), the flow generates a vortex street in the wake region. The periodic shedding of the vortices from the surface of the body induces periodic pressure variation on the body-structure. In the transverse direction, the excitation force has a dominant frequency called Karman vortex shedding frequency. In the drag direction the dominant frequency is at twice the Kaman frequency.

Furthermore, in the range of low Reynolds numbers, the signal of the drag coefficient shows multiple frequencies, while that of the lift coefficient shows the presence of only the vortex shedding frequency. The fractional harmonics in the drag signal represent larger length scales in the vorticity field and sometimes they are responsible for periodically increasing the lift amplitude beyond their nominal value.

The shedding frequencies were determined by selecting a long time trace and performing a Fourier transform operation on it. While the dominant frequency was centered around a small band, we have not analyzed variations in this frequency. Oppositely

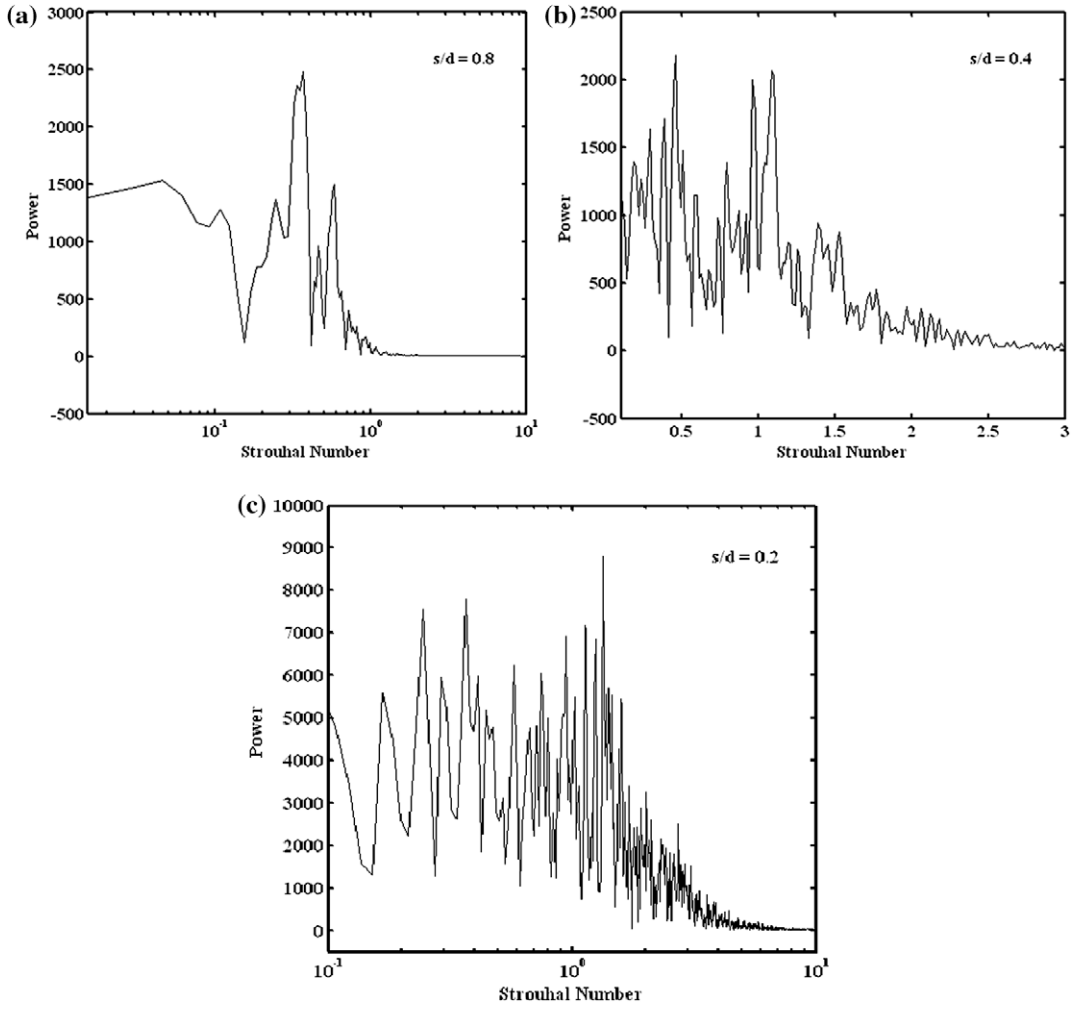

Fig. 14. Power spectrum of lift coefficient signal for $s/d < 1$: (a) s/d = 0.8, (b) s/d = 04 and (c) s/d = 0.2.

oriented vortices traveling above and below the midplane of the wake will result in a bimodal distribution of the streamwise velocity variation (oscillation) and the drag coefficient. Since the variation of the lift coefficient and that of the transverse velocity are synonymous, the fluctuations display single peak.

The vortex shedding frequency for such periodic flows where there is very little interaction between the wakes due to relative large separation ratio can be determined from the time evolution plot of the lift coefficient distribution. The time period τ can be obtained computationally by observing the non-dimensional time when the lift coefficient is just crossing the mean value. The difference between two such alternate time values gives the time period τ. Once the time period is known the corresponding frequency ($f = 1/\tau$) and the Strouhal number ($St = fd/u_\infty$) can be evaluated. Table 2 shows the mean amplitude of drag coefficient signals (λ_{CD}), phase difference between lift coefficient signals of C_1 and C_2 (φ), time period of vortex shedding (τ) and Strouhal number (St) for $s/d = 4$, 3 and 2.

Fig. 11a and b represents the time series of lift and drag coefficients for two adjoining cylinders (C_1 and C_2) for the case of $s/d = 1.2$. It is evident from these figures that the time response of drag coefficient shows more chaotic behavior than the lift coefficient. This reveals that the dynamics of lift and drag coefficients become decoupled at smaller separation ratio (Kumar et al., 2008) like $s/d = 1.2$ as has been justified from the merging of jets described above. As it is difficult to ascertain any definite value of frequency from the time signals presented in Fig. 11a and b a spectral analysis is carried out from the lift signal. The resulting power spectrum is shown in Fig. 12. The peak corresponding to the Strouhal number of 0.31 represents the primary vortex shedding frequency. Besides this primary frequency, the diffused peaks in the power spectra correspond to the combined frequencies which are culminations of the nonlinear interactions among the shed vortices of different cylinders. This combined frequency is termed as the secondary or cylinder interaction frequency (Kumar et al., 2008). The existence of this secondary or cylinder interaction frequency is mainly responsible for the chaotic nature of the lift and drag coefficient at smaller separation ratio. It should also be noted that the mean amplitude of the drag coefficient increases as the spacing between the cylinders decreases. This is because of the fact that the secondary frequency makes an increasingly dominant contribution towards the drag signal with the reduction in spacing between the cylinders (Kumar et al., 2008).

Fig. 13a–f represents the time evolution of lift and drag coefficient signals of two consecutive cylinders (C_1 and C_2) for the case of $s/d < 1$. It is interesting to note that both the instantaneous lift and drag coefficients increase rapidly with a reduction in the separation ratio and also they become more and more chaotic. This can be attributed to the fact that the wakes behind the cylinders at these small separation ratios become narrower which results a lower downstream pressure (by examining both vorticity and pressure fields at the same instant; not shown here). Consequently, the drag force is large and hence results in a larger drag coefficient, since the pressure force is the major constituent of the overall drag force. This narrower and shorter wakes interact with each other in a more chaotic fashion giving rise to the secondary frequencies

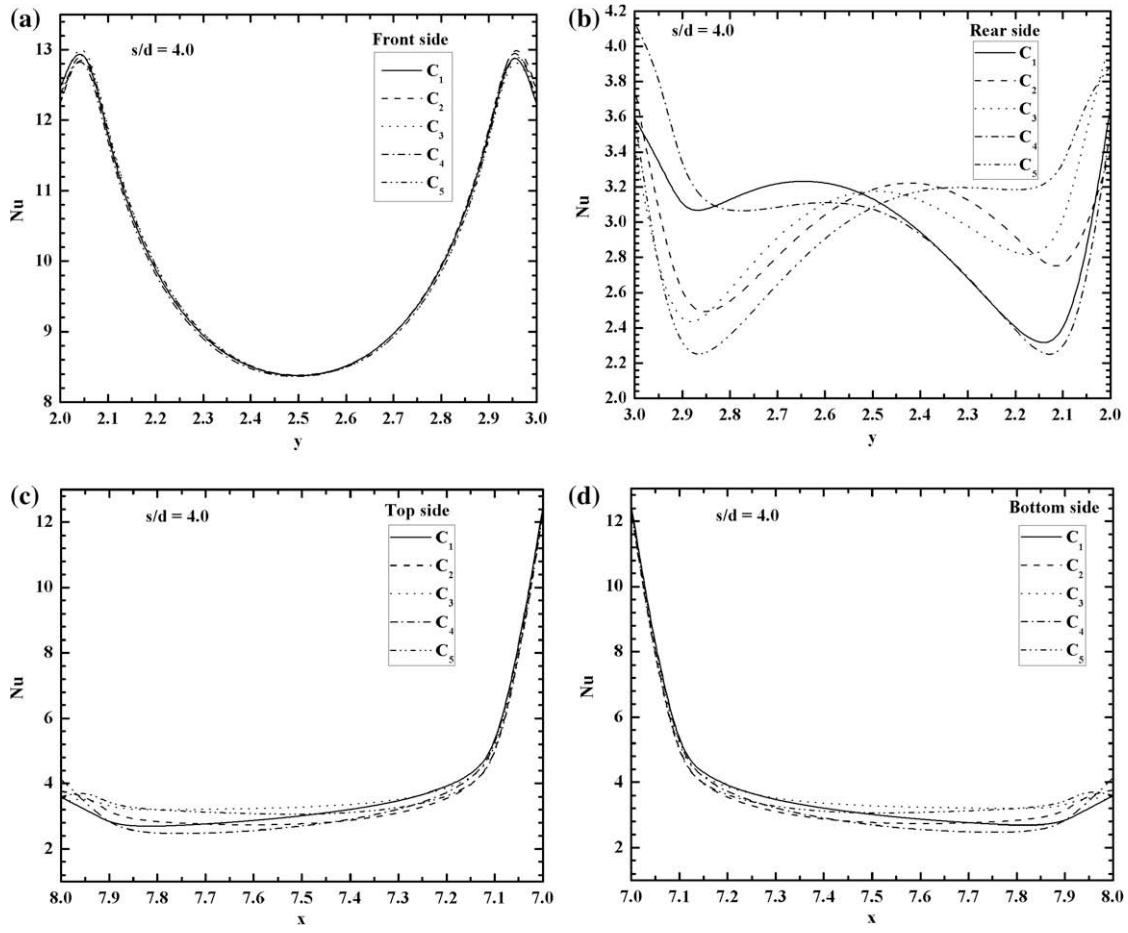

Fig. 15. Variation of instantaneous local Nusselt number for $s/d = 4$: (a) front side, (b) rear side, (c) top side and (d) bottom side.

(Kumar et al., 2008). The spectral analysis of the corresponding lift signals clearly reveals the existence of the secondary frequencies as shown in Fig. 14a–c.

The variation of instantaneous local Nusselt number for the cylinders along their different sides for the case of $s/d = 4$ is shown in Fig. 15a–d. The qualitative variations are same for all separation ratios and hence only the case of $s/d = 4$ is plotted as a representative result. As seen from Fig. 15a–d, the Nusselt number for the front surface displays much higher value than the top, bottom and rear surfaces. This is because the cold fluid impinges directly on the front faces of the cylinders which results a greater heat transfer at those faces. The front surfaces of all the cylinders also have the same distribution (qualitatively as well as quantitatively) of local Nusselt number since they experience the same undisturbed fluid (hydrodynamically and thermally). As a result of interactions in the wakes behind the cylinders and also inside the gaps between the cylinders, the local Nusselt number distribution on the rear sides and on the top and bottom surfaces of the cylinders are different. It is to be noted that the distribution is symmetric on the front surface with respect to the mid longitudinal plane through the cylinders. The corresponding Nusselt number is minimum at the midpoint and maximum close to the corners. Since the heat transfer rate is closely related to the flow field, the local heat transfer rate is minimum where the velocity magnitudes are relatively small. On the top faces of the cylinders, heat transfer decreases along the flow direction as the heat flux in the upstream is convected to the downstream by the fluid.

The time responses of local Nusselt number (for two consecutive cylinders, e.g. C_1 and C_2) for different separation ratios are shown in Fig. 16a–g. The local Nusselt number is found to oscillate

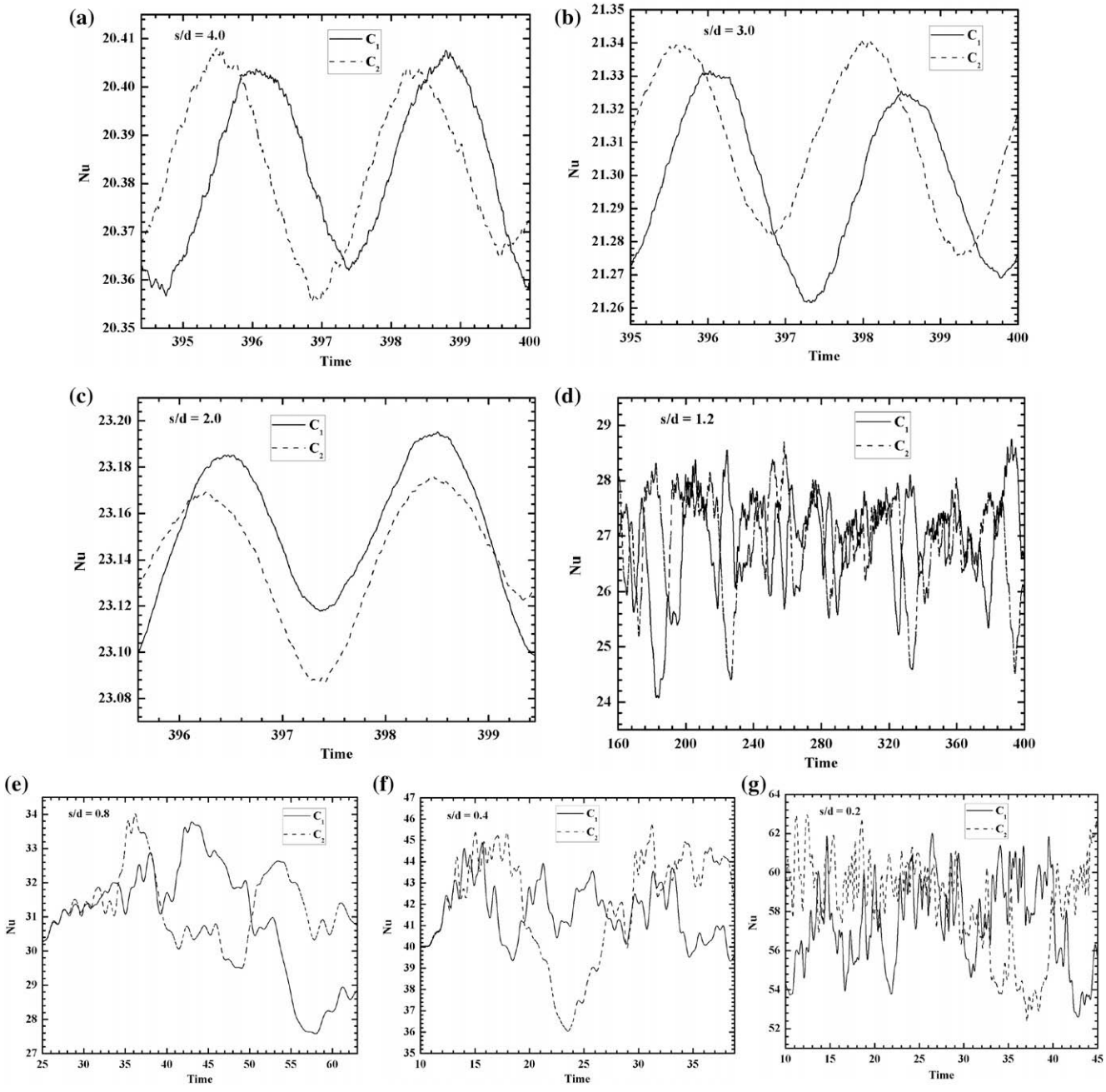

Fig. 16. Time response of local Nusselt number: (a) $s/d = 4$, (b) $s/d = 3$, (c) $s/d = 2$, (d) $s/d = 1.2$, (e) $s/d = 0.8$, (f) $s/d = 0.4$ and (g) $s/d = 0.2$.

periodically in time due to vortex shedding and a sinusoidal variation is observed for the separation ratio range of $2 \leqslant s/d \leqslant 4$. The variation becomes chaotic for smaller spacing ($0.2 \leqslant s/d \leqslant 1.2$). Consequently, the amplitude of oscillation increases with a corresponding reduction in the separation ratio. Fig. 17 is plotted in this context to show the variation of mean amplitude of oscillation of the local Nusselt number with separation ratio. The plot is shown up to $s/d = 4$, since beyond this there is no perceptible variation in the mean amplitude.

4.3. Variation of mean drag, Strouhal number and mean Nusselt number with separation ratio

The mean drag coefficient ($\overline{C}_D$) in this analysis is computed from time averaging of the signal of drag coefficients obtained for all the five cylinders. Additionally, $\overline{C}_D$ can be expressed as a function of the separation ratio (s/d) as (Kumar et al., 2008):

$$\overline{C}_D = 1.53 - \frac{1.3}{(s/d)^{0.67}} + \frac{6.6}{(s/d)^{1.34}} \tag{13}$$

The above equation will give the value of mean drag coefficient for a single cylinder ($\overline{C}_D = 1.53$) when $s/d \to \infty$. Fig. 18 shows the variation of $\overline{C}_D$ obtained from the present computation as well as from Eq. (13). The mean drag coefficient of the present computation is found to decrease with an increase in the separation ratio which is in good agreement with Eq. (13).

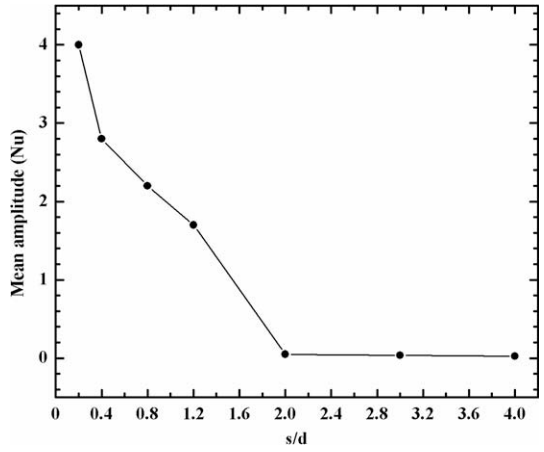

Fig. 17. Variation of mean amplitude of oscillation for local Nusselt number with separation ratio.

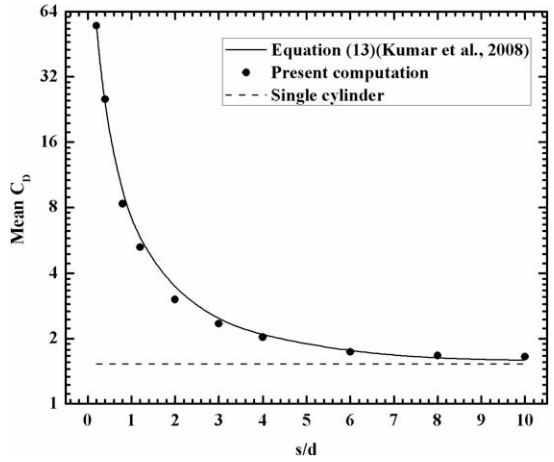

Fig. 18. Variation of mean C_D with separation ratio.

The variation of Strouhal number with the separation ratio is depicted in Fig. 19. It exhibits the same nature as that of mean drag, i.e. the Strouhal number decreases with an increase in the separation ratio. Further, the Strouhal number is computed from the empirical relation given in Kumar et al. (2008):

$$St = 0.1275 + \frac{0.1792}{s/d} \tag{14}$$

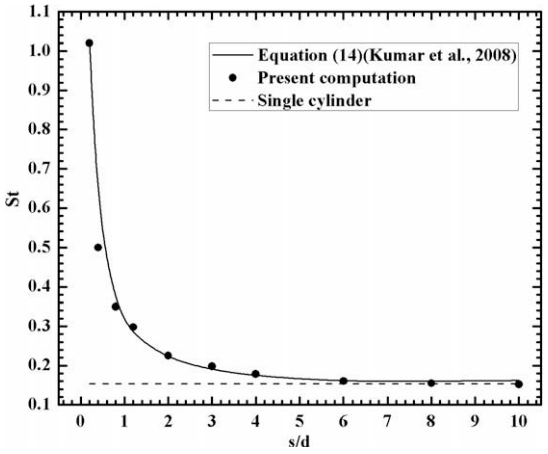

Fig. 19. Variation of Strouhal number with separation ratio.

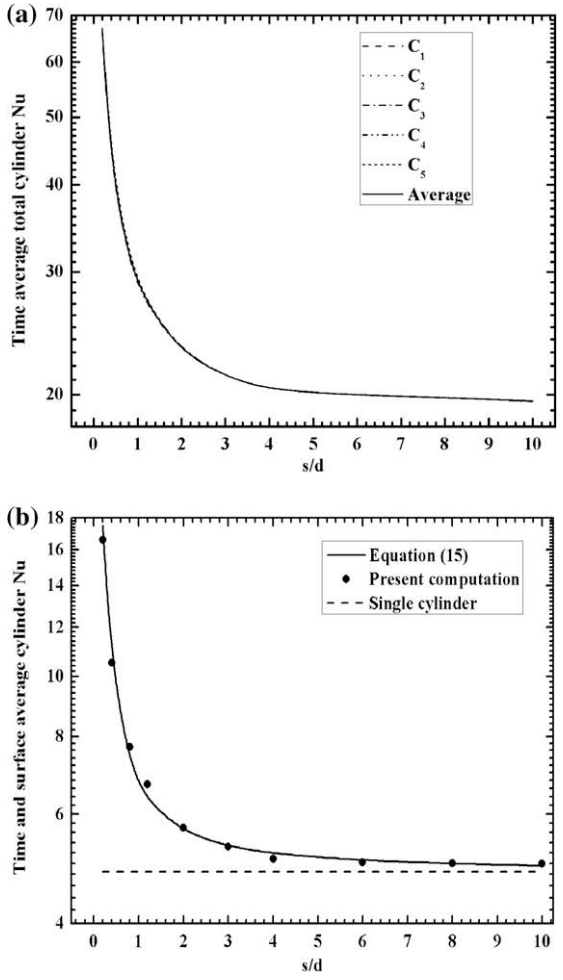

Fig. 20. Variation of Nusselt number with separation ratio: (a) time average total cylinder Nu and (b) time and surface average cylinder Nu.

The present computation matches well with Eq. (14) as shown in Fig. 19.

The variation of time average total cylinder Nusselt number and time as well as surface average cylinder Nusselt number with separation ratio are shown in Fig. 20a and b. Fig. 20a shows the Nusselt number values of all the individual cylinders and their averages for different separation ratios. As the spacing between the cylinders becomes larger, the corresponding Nusselt number becomes less. From Fig. 20b, the average Nusselt number is found to decrease with an increase in s/d and reach asymptotically the single cylinder value as $s/d \to \infty$. This behavior can be mathematically expressed by devising a new correlation between the average Nusselt number and separation ratio following the curve fitting technique using least-squares method. The following expression with a maximum deviation of 5% is proposed:

$$\overline{Nu} = 4.85 + \frac{1.7952}{(s/d)^{1.224}} \tag{15}$$

In Fig. 20b, the nature of the proposed equation (Eq. (15)) with the present computation is also compared for better visual appreciation.

5. Conclusion

A comprehensive numerical simulation for the forced convection heat transfer during flow past a row of five square cylinders placed side-by-side at different separation ratios and a fixed Reynolds number has been carried out by a finite volume method in a two-dimensional domain. The wake structure and the corresponding vortex shedding mechanism and their effects on the thermal histories are studied extensively for different spacing of the cylinders. At relatively higher separation ratios ($2 \leqslant s/d \leqslant 4$) the flow and thermal fields are dominated by the primary vortex shedding (Strouhal) frequency. The lift and drag coefficient signals obtained at these separation ratios are found to be varying in sinuous mode which also ensure that the primary frequency pertaining to the vortex shedding is the dominant frequency and there is no significant contribution of the secondary frequency. For smaller separation ratios ($0.8 \leqslant s/d \leqslant 1.2$) the vortices no longer remain distinct downstream the computational domain, because of strong interactions between the jets created by the gaps of the cylinders and the shed vortices. These interactions give rise to the secondary or cylinder interaction frequencies that are responsible for a substantial increase in mean drag coefficient and also the amplitude of lift and drag coefficients (Kumar et al., 2008). Very strong interaction between the jets and shed vortices can be found at $s/d = 0.2$ and 0.4 and hence the vortices at the near wake are found to be no longer clearly visible. The drag coefficient signal becomes more chaotic than the signal for the lift coefficient and the corresponding power spectra become broader with no preference to dominant frequency. Hence, at this configuration the flow becomes completely chaotic and a more rigorous numerical experimentation is required to capture the low-dimensional chaos at very small separation ratios.

The mean drag, Strouhal number and mean Nusselt number exhibit similar variation when represented as a function of separation ratio. All these global quantities lead asymptotically towards the corresponding single cylinder values as the separation ratio tends to the largest value considered for the present study. A novel correlation function is devised to represent the variation of the average Nusselt number with the cylinder spacing.

References

Agrawal, A., Djenidi, L., Antonia, R.A., 2006. Investigation of flow around of a pair of side-by-side square cylinders using the lattice Boltzmann method. Comput. Fluids 35, 1093–1107.

Bradshaw, P., 1965. The effect of wind-tunnel screens on nominally two-dimensional boundary layers. J. Fluid Mech. 22, 679–687.

Chatterjee, D., Biswas, G., Amiroudine, S. Numerical simulation of flow past row of square cylinders for various separation ratios. Comput. Fluids. in press doi:10.1016/j.compfluid.2009.07.002.

Inoue, O., Suzuki, Y., 2007. Beat of sound generated by flow past three side-by-side square cylinders. Phys. Fluids 19 (048102), 1–4.

Inoue, O., Iwakami, W., Hatakeyama, N., 2006. Aeolian tones radiated from flow past two square cylinders in a side-by-side arrangement. Phys. Fluids 18 (046104), 1–20.

Issa, R.I., 1986. Solution of the implicitly discretized fluid flow equations by operator splitting. J. Comp. Phys. 62, 40–65.

Kobayashi, T., 1984. Photograph Album of Flows. JSME, Maruzen, Tokyo. p. 43.

Kolar, V., Lyn, D.A., Rodi, W., 1997. Ensemble-averaged measurements in the turbulent near wake of two side-by-side square cylinders. J. Fluid Mech. 346, 201–237.

Kumar, S.R., Sharma, A., Agrawal, A., 2008. Simulation of flow around a row of square cylinders. J. Fluid Mech. 606, 369–397.

Mizushima, J., Akinaga, T., 2003. Vortex shedding from a row of square bars. Fluid Dyn. Res. 32, 179–191.

Mizushima, J., Takemoto, Y., 1996. Stability of the flow past a row of square bars. J. Phys. Soc. Jpn. 65, 1673–1685.

Morgan, V.T., 1975. The overall convective heat transfer from smooth circular cylinders. Adv. Heat Transfer. 11, 199–264.

Mukhopadhyay, A., Biswas, G., Sundararajan, T., 1992. Numerical investigation of confined wakes behind a square cylinder in a channel. Int. J. Numer. Methods. Fluids 14, 1473–1484.

Robichaux, J., Balachandar, S., Vanka, S.P., 1999. Two-dimensional Floquet instability of the wake of square cylinder. Phys. Fluids 11, 560–578.

Sewatkar, C.M., Sharma, A., Agrawal, A., 2009. On the effect of Reynolds number for flow around a row of square cylinders. Phys. Fluids 21, 083602.

Sharma, A., Eswaran, V., 2004. Heat and fluid flow across a square cylinder in the two-dimensional laminar flow regime. Numer. Heat Transfer A 45, 247–269.

Shimizu, Y., Tanida, Y., 1978. Fluid forces acting on cylinders of rectangular cross section. Transc JSME B 44, 2699–2706.

Sohankar, A., Etminan, A., 2008. Forced-convection heat transfer from tandem square cylinders in cross flow at low Reynolds numbers. Int. J. Numer. Methods Fluids. doi:10.1002/fld.1909.

Sohankar, A., Norberg, C., Davidson, L., 1997. Numerical simulation of unsteady low-Reynolds number flow around rectangular cylinders at incidence. J. Wind Eng. Ind. Aerodyn. 69, 189–201.

Sohankar, A., Norberg, C., Davidson, L., 1998. Low-Reynolds-number flow around a square cylinder at incidence: study of blockage, onset of vortex shedding and outlet boundary condition. Int. J. Numer. Methods Fluids 26, 39–56.

Sumner, D., Wong, S.S.T., Price, S.J., Paidoussis, M.D., 1999. Fluid behavior of side-by-side circular cylinders in steady cross-flow. J. Fluids Struct. 13, 309–338.

Suzuki, K., Suzuki, H., 1994. Unsteady heat transfer in a channel obstructed by an immersed body. Annu. Rev. Heat Transfer 5, 177–206.

Valencia, A., Cid, M., 2002. Turbulent unsteady flow and heat transfer in channels with periodically mounted square bars. Int. J. Heat Mass Transfer 45, 1661–1673.

Williamson, C.H.K., 1985. Evolution of a single wake behind a pair of bluff bodies. J. Fluid Mech. 159, 1–18.

Zdravkovich, M.M., 1997. Flow Around Circular Cylinders: Fundamentals, vol. 1. Oxford University Press, New York.

Zdravkovich, M.M., 2003. Flow Around Circular Cylinders: Applications, vol. 2. Oxford University Press, New York.

Zhou, Y., So, R.M.C., Liu, M.H., Zhang, H.J., 2000. Complex turbulent wakes generated by two and three side-by-side cylinders. Int. J. Heat Fluid Flow 21, 125–133.